Compressional Alfvén and ion-ion hybrid modes in the deuterium-tritium plasma of a spherical tokamak power plant

M. K. Lilley[a)]
Department of Plasma Physics, Imperial College, London SW7 2AZ, United Kingdom

S. E. Sharapov
EURATOM/UKAEA Fusion Association, Culham Science Centre, Abingdon OX14 3DB, United Kingdom

(Received 15 March 2007; accepted 4 June 2007; published online 15 August 2007)

A discrete spectrum of compressional Alfvén eigenmodes and ion-ion hybrid eigenmodes is found to exist above the tritium ion cyclotron frequency in the deuterium-tritium (D-T) plasma of a spherical tokamak power plant (STPP) [H. R. Wilson *et al.*, *19th IAEA Fusion Energy Conference* (IAEA, Lyon, France, 2002), No. FT/1-4]. An equilibrium magnetic well formed in a STPP, as a result of plasma diamagnetism, causes all externally launched electromagnetic waves to propagate from the side of high total magnetic field, and it is this well that forms discrete spectra in the ion cyclotron resonance heating frequency range near the plasma core. The eigenmodes, as well as the position of the mode conversion layers, are obtained in a one-dimensional magnetic field geometry [S. C. Cowley *et al.*, Phys. Fluids B **3**, 2066 (1991)], relevant for the STPP, which will necessarily operate at high β. The possibility of using the discrete spectrum probed with an external antenna, or driven by energetic ions, for measuring the D-T mixture ratio is discussed. © *2007 American Institute of Physics*. [DOI: 10.1063/1.2752824]

I. INTRODUCTION AND BACKGROUND

The success of the spherical tokamak, with inverse aspect ratio $a/R \approx 0.7$, where a and R are the minor and major radii of the torus, respectively, has led to the start of the design of a spherical tokamak power plant (STPP) with $a/R=0.713$.[1] The main advantages of a spherical tokamak are the following:

- Enhanced plasma stability due to the higher ratio of magnetic field on the inboard (high magnetic field) to outboard (low magnetic field) side of the tokamak, which implies a greater average stabilizing curvature, as compared to conventional (small inverse aspect ratio) tokamaks.
- As a result of better magnetohydrodynamic (MHD) stability, a higher limit of $\beta=2\mu_0 P/B_0^2$, desirable for fusion, can be achieved.[2] The β value in spherical tokamaks can be up to an order of magnitude higher than in conventional tokamaks, e.g., a record volume averaged toroidal β (β_t) of 40% was achieved on START in Culham,[3] the National Spherical Torus Experiment achieved $\beta_t \sim 35\%$,[4] and the predicted β_t for STPPs is 59%.[1]

Electromagnetic (EM) instabilities are often excited in present-day spherical tokamaks (STs), driven by energetic ions produced by neutral beam injection (NBI) with $V_{\mathrm{NBI}} > V_A$ (here V_{NBI} is the velocity of the beam, $V_A=B_0/\sqrt{\mu_0\rho}$ is the Alfvén speed, and B_0 and ρ are the equilibrium magnetic field and plasma mass density, respectively).[5,6] In a STPP, there will be a significant population of alpha particles, born in deuterium-tritium (D-T) fusion reactions at an energy of 3.52 MeV, which could drive EM instabilities. This is one of the important issues facing STPP's. Because of the high β in STPP's, these energetic particle driven EM instabilities will differ significantly from fusion power plants derived from conventional tokamaks with typical inverse aspect ratio $a/R \approx 0.3$ and $\beta \approx 1-5\%$, in which instabilities in the Alfvén frequency range (e.g., toroidal Alfvén eigenmodes) are considered to be most dangerous. More specifically for $\beta \approx 1$ (valid in the plasma core of a STPP), EM instabilities in the Alfvén frequency range will be strongly damped by interaction with thermal ions via Landau resonance ($V_A \approx V_{\|i}$), where $V_{\|i}=\mathbf{V_i}\cdot\mathbf{B}_0/|\mathbf{B}_0|$ is the parallel velocity of the thermal ions. On the other hand, instabilities of higher frequency ω comparable to the ion cyclotron frequency ω_{ci}, excited via cyclotron resonances, $\omega=k_\| v_{\|\alpha}-l\omega_{c\alpha}$ (here $k_\|=\mathbf{k}\cdot\mathbf{B}_0/|\mathbf{B}_0|$ and l is an integer), will be relevant, since Landau resonance for thermal ions involves the phase velocity $\omega/k_\|$, which can differ significantly from the thermal ion speed. These instabilities may involve compressional Alfvén eigenmodes, shear Alfvén eigenmodes[7] with finite ratio ω/ω_{ci}, and ion-ion hybrid eigenmodes.[8] They may be driven by free energy sources associated with gradients in velocity space of the α particle distribution function, and cause nonclassical relaxation of the α particles in velocity space.

The aim of the present paper is to investigate a discrete EM spectrum, in the ion cyclotron frequency range, which may be driven by fusion born alpha particles or scanned with an external antenna for diagnostic purposes similar to Ref. 8, in D-T plasma of a STPP.[1] Due to the large Shafranov shift and high-β, STs contain a well in the equilibrium magnetic field on the outboard side of the torus. In addition, the mixture of D-T ions gives rise to ion-ion hybrid effects.[9] Such a magnetic well in $|\mathbf{B}_0|(R)$, together with D-T effects, significantly changes the properties of the EM propagation as compared to the conventional tokamaks with a monotonic $|\mathbf{B}_0|(R)$ profile operating in deuterium only. This is due to the change

a)Electronic mail: m.lilley@imperial.ac.uk

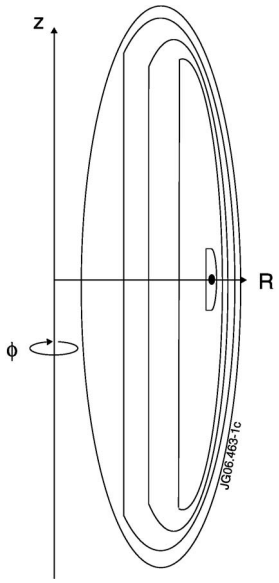

FIG. 1. Elliptical ST plasma with D-shaped flux surfaces. There exists a "core" region of the plasma where these flux surfaces are 1D, and there exists a narrow "boundary layer" where the curvature is important (the black dot represents the "magnetic axis").

of radial position of cutoffs and mode conversion layers, so waves launched from the outboard side in a STPP are always propagating from the side of high total magnetic field $|\mathbf{B}_0|$, in contrast to most present day conventional tokamaks. In the subsection entitled "The eigenvalue equation" in Sec. II and in Sec. III, we investigate the role this magnetic well can have as a resonating cavity for EM waves, since the inhomogeneities in the magnetic field form reflection points inside the plasma and hence a localized eigenmode structure is possible.[10] Most attention is paid to the frequency range between the cyclotron frequencies of deuterium and tritium at the minimum of $|\mathbf{B}_0|$, where the effect of D-T concentration on the frequency is strongest.

Wave propagation is analyzed using the "cold plasma" approximation,[11] and by assuming that the perturbed electric field $\mathbf{E}$ only has components perpendicular to the equilibrium magnetic field, the "cold plasma" vector wave equation is reduced to two components for $\mathbf{E}$. These equations will be the subject of our analysis for a STPP.

It has been shown[12] that high β tokamak plasmas have essentially a 1D magnetic field structure in the core of the plasma (i.e., the flux surfaces are accurately modeled by straight vertical lines), and so provide slowly varying equilibrium parameters in the vertical direction [e.g., $\varepsilon=\varepsilon(R)$ in the plasma core, where ε is the dielectric tensor], as illustrated by Fig. 1.

An ordering is therefore applied, whereby the perturbed variables are assumed to vary on a much shorter vertical scale than the equilibrium quantities. This simplifies the cold plasma vector wave equation into one equation for one of the components of the perpendicular electric field as a function of major radius alone, i.e., we have a one-dimensional (1D) eigenvalue equation to solve. In contrast to the analysis in Ref. 10, this paper includes deuterium-tritium (D-T) effects, a more complete treatment of the equilibrium magnetic field and nonzero refractive index $N_\parallel = ck_\parallel/\omega$ parallel to the equilibrium magnetic field.

II. THE WAVE EQUATION AND THE DIELECTRIC TENSOR

Faraday's and Ampère's laws, along with the assumption of harmonic fields and currents of the wave (i.e., $\mathbf{X}=\mathbf{X}_0 e^{-i\omega t}$, where $\mathbf{X}$ can be current $\mathbf{J}$ or electric or magnetic field, $\mathbf{E}$ or $\mathbf{B}$), lead to the general wave equation[13]

$$\nabla \times \nabla \times \mathbf{E} = \frac{\omega^2}{c^2}\varepsilon \mathbf{E}, \tag{1}$$

where $\varepsilon = I + i\sigma/\epsilon_0\omega$ is the dielectric tensor and σ is the electrical conductivity tensor. By considering the "cold plasma" approximation, where the frequency ω of the wave is much greater than the electron ion collision frequency ν_{ei}, and the phase velocity ω/k is much greater than the thermal speed of the ions V_{Ti} and electrons V_{Te},

$$\nu_{ei} \ll \omega, \quad V_{Te}, V_{Ti} \ll \frac{\omega}{k}$$

[such a description is also valid for $V_{Ti} \ll \omega/k \ll V_{Te}$ (Ref. 13)] with the following set of equations describing plasma dynamics:

$$\mathbf{J} = \sum_\alpha e_\alpha n_\alpha \mathbf{v}_\alpha, \tag{2a}$$

$$\frac{d\mathbf{v}_\alpha}{dt} = \frac{e_\alpha}{m_\alpha}(\mathbf{E} + \mathbf{v}_\alpha \times \mathbf{B}_0), \tag{2b}$$

one finds the form of ε to be[13]

$$\varepsilon = \begin{pmatrix} \varepsilon_1 & i\varepsilon_2 & 0 \\ -i\varepsilon_2 & \varepsilon_1 & 0 \\ 0 & 0 & \varepsilon_3 \end{pmatrix}. \tag{3}$$

For the 1D equilibrium geometry of the STPP plasma core,

$$\varepsilon_1(R,\omega) = 1 - \sum_\alpha \frac{\omega_{p\alpha}^2(R)}{\omega^2 - \omega_{c\alpha}^2(R)},$$

$$\varepsilon_2(R,\omega) = -\sum_\alpha \frac{\omega_{c\alpha}(R)}{\omega}\frac{\omega_{p\alpha}^2(R)}{\omega^2 - \omega_{c\alpha}^2(R)}, \tag{4}$$

$$\varepsilon_3(R,\omega) = 1 - \sum_\alpha \frac{\omega_{p\alpha}^2(R)}{\omega^2}, \quad \alpha = D,T,e.$$

For frequencies of interest here, $\omega \ll \omega_{pi}, \omega_{pe}$, the dielectric tensor elements $\varepsilon_1, \varepsilon_2$ take the following form:

$$\varepsilon_1(R,\omega) \approx \varepsilon_{1D}(R,\omega) + \varepsilon_{1T}(R,\omega),$$

$$\varepsilon_2(R,\omega) \approx \frac{\omega}{\omega_{cD}(R,\omega)}\varepsilon_{1D}(R,\omega) + \frac{\omega}{\omega_{cT}(R,\omega)}\varepsilon_{1T}(R,\omega), \tag{5}$$

$$\varepsilon_{1D}(R,\omega) = -\frac{\omega_{pD}^2(R,\omega)}{\omega^2 - \omega_{cD}^2(R,\omega)},$$

$$\varepsilon_{1T}(R,\omega) = -\frac{\omega_{pT}^2(R,\omega)}{\omega^2 - \omega_{cT}^2(R,\omega)}.$$

Due to the two ion terms in Eq. (5), the behavior of ε_1 in D-T is different from that of a single ion species plasma (where only one term is present). The main consequences are that both the cutoff and mode conversion positions change, affecting the eigenfrequency and damping of the EM modes. Note that the fraction of tritium $\kappa_T = n_T/n_e$ relative to that of deuterium $\kappa_D = n_D/n_e$ will be an important factor in just how much of an effect the dual ion species plasma will have on the EM waves. We consider the effect of changing κ_T on the EM wave in the approximation that κ_T does not vary with radius.

The eigenvalue equation

By considering Eqs. (1) and (3) for a spherical tokamak, the following right-handed set of coordinates should be used: (R,z,ϕ). Equation (1) is now considered as an eigenvalue equation to be solved for eigenfrequency ω. To simplify the analysis, we focus only on the eigenmodes created through inhomogeneity of $|\mathbf{B}_0|$, and so keep the plasma density, and hence ω_{pi}, constant. To this end, we appeal to a paper by Gorelenkova *et al.* and follow the technique used in their analysis.[10]

First, infinite electrical conductivity parallel to the magnetic field, i.e., $\varepsilon_3 \to \infty$ in the "cold plasma" model, implies that the third component of Eq. (1) is

$$E_\phi = E_\parallel = 0 \tag{6}$$

(note by $\parallel$ we mean parallel to the equilibrium magnetic field $E_\parallel = \mathbf{E}\cdot\mathbf{B}_0/|\mathbf{B}_0|$). The two projections of Eq. (1) perpendicular to $\mathbf{B}_0$ can be written as[10]

$$-\left(\frac{\partial^2}{\partial z^2} + F\right)E_R + \left(\frac{\partial^2}{\partial R \partial z} - H\right)E_z = 0, \tag{7a}$$

$$\left(\frac{\partial^2}{\partial R \partial z} + \frac{1}{R}\frac{\partial}{\partial z} + H\right)E_R - \left(\frac{\partial^2}{\partial R^2} + \frac{1}{R}\frac{\partial}{\partial R} + F\right)E_z = 0 \tag{7b}$$

with $F = (\omega^2/c^2)\varepsilon_1, H = i(\omega^2/c^2)\varepsilon_2$, where "i" in the definition of H has been corrected from the misprint in Ref. 10.

Papers by Cowley *et al.*[12,14] demonstrated that high beta tokamak equilibria are inherently 1D in the core region of the plasma (as illustrated by Fig. 1). This naturally leads to the use of the following assumption in Eq. (7): $\partial \ln B/\partial z \ll \partial \ln E_{R,z}/\partial z$, which physically says that the equilibrium plasma variables vary slowly in the vertical direction compared to the perturbations.[10] This gives

$$\left(\frac{\partial^2}{\partial z^2} + \frac{1}{R}\frac{\partial}{\partial R}R\frac{\partial}{\partial R} + \frac{F^2+H^2}{F} + \frac{H}{RF}\frac{\partial}{\partial z}\right)E_z = 0, \tag{8}$$

where $1/R$ in the last term has been corrected from the misprint in Ref. 10. Note that Ref. 10 does not include the case $N_\parallel \neq 0$. In order to include this, we renormalize F as $\varepsilon_1 \to \varepsilon_1 - N_\parallel^2$,

$$F = \frac{\omega^2}{c^2}(\varepsilon_1 - N_\parallel^2), \tag{9}$$

then the derivation of the eigenvalue equation for E_z follows the same as in Ref. 10 (note we have assumed that $N_\parallel$ is not a function of position in the plasma). In order to simplify Eq. (8) further, we use an approximation from Ref. 10,

$$E_z(R,z) \simeq \hat{E}_z(R)e^{ilz/\Delta_z}, \tag{10}$$

so one considers $\partial/\partial z \to ik_z$ (where Δ_z represents a characteristic vertical magnetic well depth and l is an integer). Finally, by taking E_z to be of the following form:

$$E_z = A(R)R^{-1/2}, \tag{11}$$

one obtains [from Eq. (8)] an equation with second-order derivatives of A,

$$\left(\frac{\partial^2}{\partial R^2} - V\right)A = 0,$$
$$V = \frac{l^2}{\Delta_z^2} + \frac{l}{\Delta_z R}\frac{\varepsilon_2}{\varepsilon_1 - N_\parallel^2} - \frac{\omega^2}{c^2}\left[\varepsilon_1 - N_\parallel^2 - \frac{\varepsilon_2^2}{\varepsilon_1 - N_\parallel^2}\right] - \frac{1}{4R^2}, \tag{12}$$

where we associate V with a potential of the Schrödinger-like equation (12). If one takes the Wentzel-Kramers-Brillouin (WKB, small wavelength or geometric optics) limit, then $k_R^2 = -V$ (where k_R is the radial component of the wave vector) and $k_R(R) = 0$ are the cutoff positions. Therefore, we would expect radially localized eigenmodes to exist (even in the non-WKB limit) if we have at least one point in the plasma where $V = 0$. The difference between Eq. (12) and the potential V from Ref. 10 is that we have not used any high-frequency approximation, and have included $N_\parallel$.

It can be seen in Eq. (12) that V has a singularity when $\varepsilon_1 = N_\parallel^2$. This singularity is associated with a mode conversion, which is an important factor in Alfvén wave damping (and hence plasma heating[15]). Equation (12) gives us information on the frequency and structure of any eigenmodes supported by the plasma consistent with our approximations. The next stage is to quantitatively analyze Eq. (12) for a STPP equilibrium.

III. STPP EQUILIBRIUM AND QUANTITATIVE ANALYSIS

We use a STPP equilibrium (Fig. 2) from the equilibrium code "SCENE."[16] Figure 3 shows the total magnetic field $|\mathbf{B}_0|$ from "SCENE" together with a polynomial fit of degree 8 used in further analysis here.

To solve Eq. (12), we expand V around $R = \tilde{R}$, where $\tilde{R}$ corresponds to a radius at which V achieves a local minimum, and keep terms up to quadratic order. Equation (12) then reduces to

$$\frac{\partial^2 A}{\partial R^2} - \left\{V(\tilde{R}) + \frac{1}{2}(R-\tilde{R})^2 \left.\frac{\partial^2 V}{\partial R^2}\right|_{(\tilde{R})}\right\}A = 0. \tag{13}$$

Equation (13) uses the harmonic-oscillator approximation to the potential V, and is the form used by Gorelenkova[10] to solve the eigenvalue equation. By using

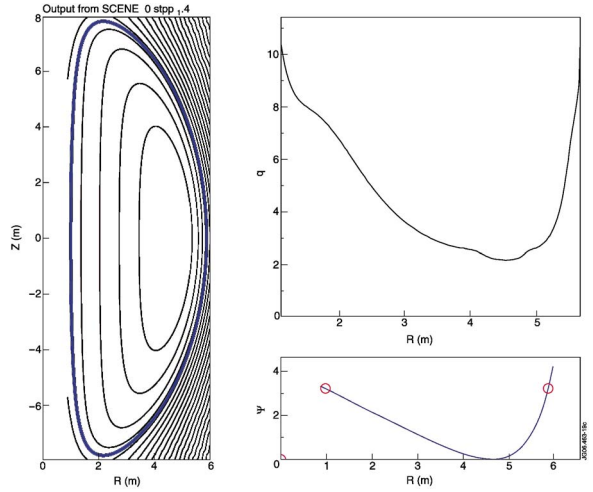

FIG. 2. (Color online) 1D nature of the flux surfaces in the core of the plasma, along with the safety factor q and flux function Ψ as functions of major radius R (data obtained from "SCENE").

well known solutions to the Schrödinger equation with a harmonic potential,[17] one can manipulate Eq. (13) into the correct form and find solutions for the frequency ω. However, from Fig. 3 one can clearly see the asymmetrical nature of the magnetic field, and hence the potential V. We therefore seek an analytical method that captures this asymmetry, such as the following Schrödinger equation, which utilizes an asymmetric potential:[17]

$$A'' + (\alpha - Be^{2ax} + 2Be^{ax})A = 0, \tag{14}$$

where $x=R-\tilde{R}$ and α, a and B are to be determined so that Eq. (13) can be written in the form of Eq. (14). First, by rewriting the potential V (by bringing the constant part out) as

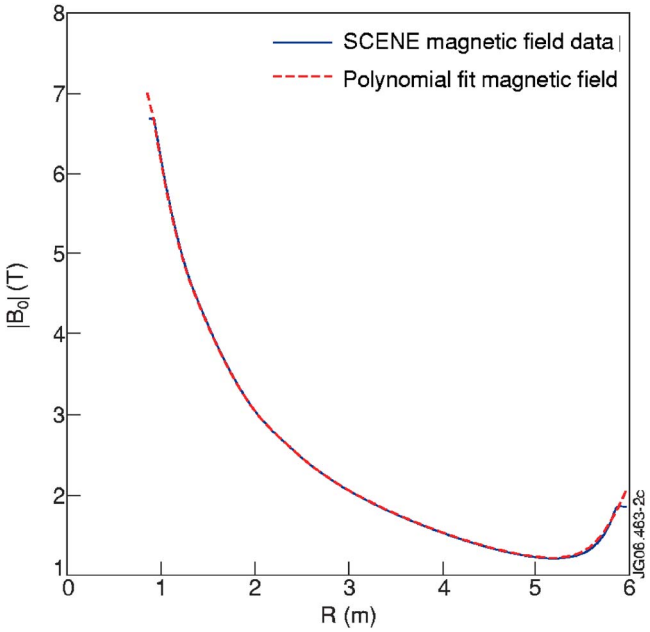

FIG. 3. (Color online) Magnetic field profile to be used in our analysis (dashed), and the original SCENE data for the total magnetic field (solid).

$$V = \frac{l^2}{\Delta_z^2} + \tilde{V},$$

$$\tilde{V} = \frac{l}{\Delta_z R}\frac{\varepsilon_2}{\varepsilon_1 - N_\parallel^2} - \frac{\omega^2}{c^2}\left[\varepsilon_1 - N_\parallel^2 - \frac{\varepsilon_2^2}{\varepsilon_1 - N_\parallel^2}\right] - \frac{1}{4R^2},$$

Eq. (13) can then be rewritten as

$$\frac{\partial^2 A}{\partial R^2} - \left\{\frac{l^2}{\Delta_z^2} + \tilde{V}(\tilde{R}) + \frac{1}{2}(R-\tilde{R})^2 \left.\frac{\partial^2 \tilde{V}}{\partial R^2}\right|_{(\tilde{R})}\right\} A = 0. \tag{15}$$

Second, we notice that, from Eq. (14), a Taylor expansion of $U=Be^{2ax}-2Be^{ax}$ about $R=\tilde{R}$ up to second order yields

$$U \approx -B + Ba^2(R-\tilde{R})^2. \tag{16}$$

Finally, by comparing Eqs. (14)–(16), we can write Eq. (13) in the form of Eq. (14) by defining the following:

$$\alpha = -\frac{l^2}{\Delta_z^2}, \quad -\tilde{V} = B, \quad a = \left(\frac{-\frac{1}{2}\left.\partial^2\tilde{V}/\partial R^2\right|_{\tilde{R}}}{\tilde{V}(\tilde{R})}\right)^{1/2}. \tag{17}$$

The eigenvalues of Eq. (14) have the following solution:[17]

$$-\alpha = B\left[1 + \frac{a}{\sqrt{B}}\left(p + \frac{1}{2}\right)\right]^2 \tag{18}$$

and the eigenfunctions have the following form:[17]

$$A = Ce^{-\xi/2}\xi^s w(\xi), \tag{19}$$

where

$$\xi = \frac{2\sqrt{B}}{a}e^{a(R-\tilde{R})}, \quad s = \frac{\sqrt{B}}{a} - p - \frac{1}{2}, \quad (p = 0,1,2,\ldots).$$

$w(\xi)$ is the confluent hypergeometric function: $w=F(-p,2s+1,\xi)$, and positive s has to be taken so that $\sqrt{B}/a > p+1/2$, C is an arbitrary constant. The eigenfrequencies are then found by solving the following equation for ω:

$$\frac{l^2}{\Delta_z^2} = -\tilde{V}(\tilde{R})\left[1 + \frac{1}{|\tilde{V}(\tilde{R})|}\left(\frac{1}{2}\left.\frac{\partial^2\tilde{V}}{\partial R^2}\right|_{\tilde{R}}\right)^{1/2}\left(p + \frac{1}{2}\right)\right]^2. \tag{20}$$

For typical values of $N_\parallel^2=10000$, $\kappa_T=0.5$ and $l=10$, $\Delta_z=0.6$ consistent with Ref. 10, we find multiple frequencies for each value of p, four in total (labeled from ω_1 to ω_4). Table I shows frequencies that have been calculated using the above approach, assuming that $\tilde{R}=5.19m$, which is a good approximation (see Fig. 3). All frequencies ω_1 and frequencies ω_2 (for $p=0,1$) correspond to ion-ion hybrid eigenmodes, while ω_2 (for $p=2$) and all of frequencies ω_3 and ω_4 correspond to compressional Alfvén eigenmodes. The internal consistency of the calculated frequencies with our method can now be checked. There is a region of applicability of the asymmetric method that must be adhered to, due to the square root in the definition of "a" in Eq. (17). Figure 4 indicates the region of applicability of the asymmetric method. At the minimum of the potential, the second derivative is always positive, which means that if $\tilde{V}(\tilde{R})$ is positive,

TABLE I. Angular frequencies, normalized to the minimum cyclotron frequency of tritium $\omega_{cT}(\tilde{R})=3.8537\times10^7$ rad s^{-1}, calculated using the Taylor expansion method with an asymmetric potential for $N_\parallel^2=10000$ and $\kappa_T=0.5$. Note that the minimum cyclotron frequency of deuterium is $\omega_{cD}(\tilde{R})=5.7805\times10^7$ rad s^{-1}.

p	ω_1	ω_2[a]	ω_3	ω_4
0	1.022	1.312	2.370	2.957
1	1.137	1.372	2.166	2.945
2	1.265	1.576	1.839	2.926

[a]In fact, two solutions of Eq. (20) exist for two closely spaced frequencies, however only one frequency can be resolved since $\Delta\omega/\omega_2<1\%$.

then "a" will not be real, and the method will not be valid. Figure 4 indicates the regions where $\tilde{V}(\tilde{R})<0$ and hence where the asymmetric method can be applied. ω_1 for $p=2$ fails to satisfy this condition and so is not consistent with our model. Although $\tilde{V}(\tilde{R})<0$ is true for all other frequencies in Table I, we must also check that the original potential ($V=l^2/\Delta_z^2+\tilde{V}$) is negative at its minimum so that our modes are physical. All the ω_4 fail to satisfy this criterion. Furthermore, these frequencies fail to satisfy a necessary condition for our model ($\sqrt{B}/a>p+1/2$), and so these frequencies are also not consistent with our model.

Now that we have calculated a few frequencies with this method, a comparison of the asymmetric and harmonic approximations can be made. We first plot the full potential along with the harmonic one from Eq. (13). The asymmetric potential is plotted by taking Eq. (15) and approximating the $\tilde{V}$ parts by U [consistent with Eq. (16)]; see Fig. 5. Now although Fig. 5 appears to suggest the asymmetric method is a better approximation than the harmonic one, Fig. 6 implies the harmonic potential is a better fit to the full potential on the inboard side, and the asymmetric is a better fit to the full potential at the outboard side. However, the nature of the asymmetry will have an effect on the structure of the perturbed electric field. In the harmonic case, the eigenfunction is centered about the minimum in the potential, however in the asymmetric case it is skewed somewhat, meaning that a larger part of the wave eigenfunction can penetrate into the mode conversion layer $\varepsilon_1=N_\parallel^2$. Figures 7 and 8 show the potential and $p=0$ eigenfunctions for the asymmetric method corresponding to Figs. 5 and 6. Note that, since our method of calculating the electric field perturbation uses an approxi-

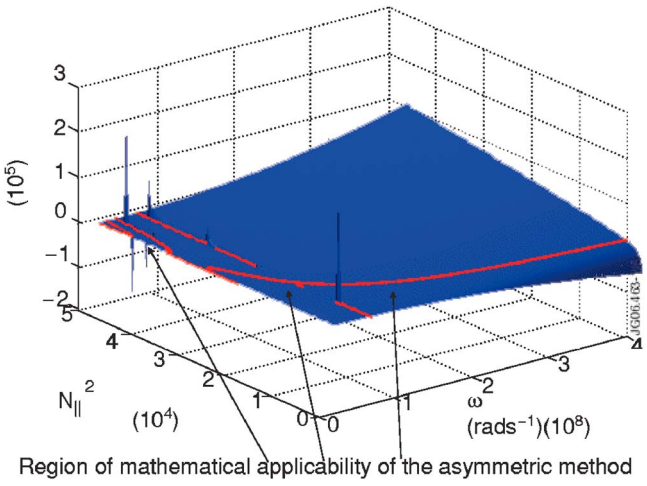

FIG. 4. (Color online) Plot of $\tilde{V}(\tilde{R})$ as a function of ω and $N_\parallel^2$ for $\kappa_T=0.5$. The line on the surface indicates the zeros of the function, and hence shows the boundaries of regions where we can and cannot apply the asymmetric method. Note the spikes in this figure are as a result of $\varepsilon_1=N_\parallel^2$.

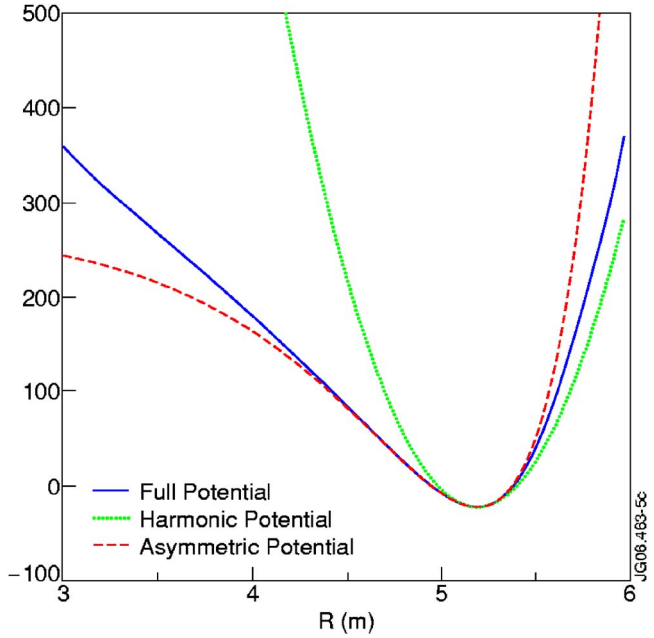

FIG. 5. (Color online) Full potential along with the corresponding harmonic and asymmetric approximations for $\kappa_T=0.5$, $N_\parallel^2=10000$, and $\omega=3.9399\times10^7$ rad s^{-1}.

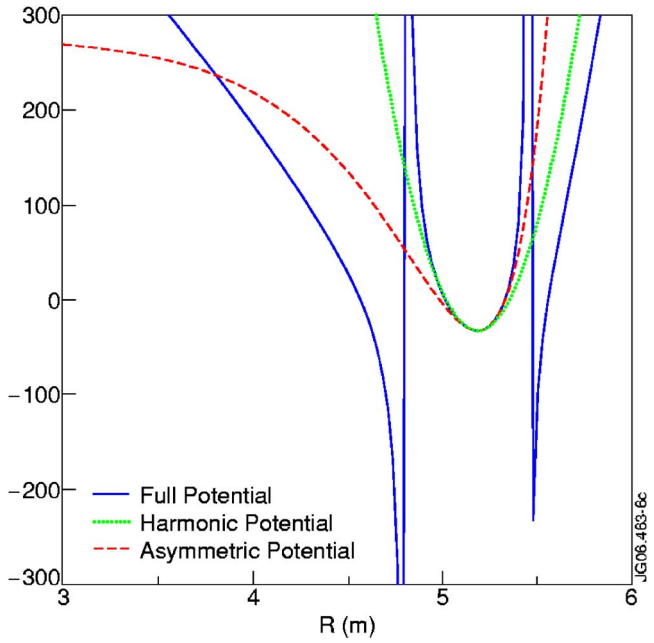

FIG. 6. (Color online) Full potential along with the corresponding harmonic and asymmetric approximations for $\kappa_T=0.5$, $N_\parallel^2=10000$, and $\omega=5.0579\times10^7$ rad s^{-1}. Note the spikes in this figure are a result of the mode conversion layer $\varepsilon_1=N_\parallel^2$.

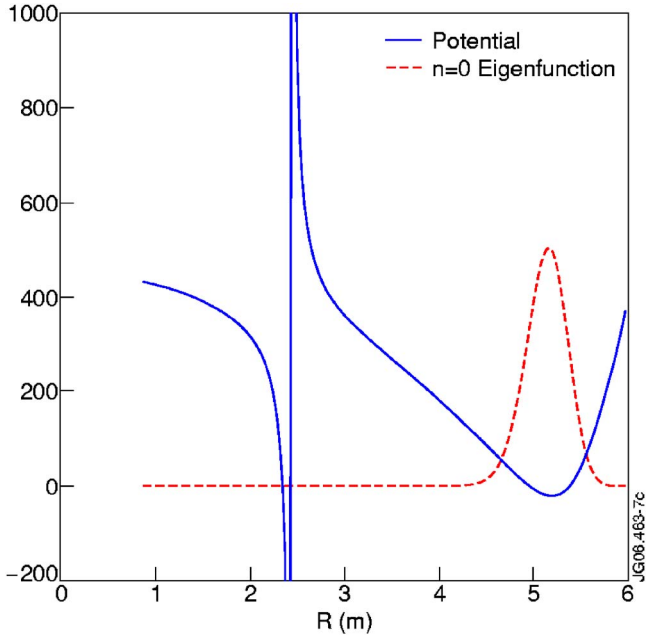

FIG. 7. (Color online) Full potential along with the z component of the electric field corresponding to the $p=0$ eigenfunction (plotted in arbitrary units) for $\kappa_T=0.5$, $N_\parallel^2=10000$, and $\omega=3.9399\times10^7$ rad s^{-1}. Note the spikes in this figure are a result of the mode conversion layer $\varepsilon_1=N_\parallel^2$.

mate potential that does not include the mode conversion points, no singularities appear in the electric field of Fig. 8. A more complete method for calculating the eigenfunctions would include this.

As can be seen from Refs. 18 and 19, the proximity of the mode conversion layer to the eigenfunction provides a damping mechanism, since the ion Bernstein waves resulting from the mode conversion are heavily damped. The distance between the mode localization region and the mode conversion layer is thus an important parameter in determining the rate of mode conversion, and hence damping, which can be calculated in accordance with Refs. 18 and 19. Figure 7 shows an example of a weakly damped mode, whereas Fig. 8 shows a mode that is expected to be heavily damped due to the mode conversion. It is not the intention of the authors to give a detailed calculation of the damping of the eigenmodes due to mode conversion. The intention is, however, to investigate the mode conversion positions for modes of different frequency to indicate frequency regimes where mode conversion will be important; this will therefore be the focus of the next section.

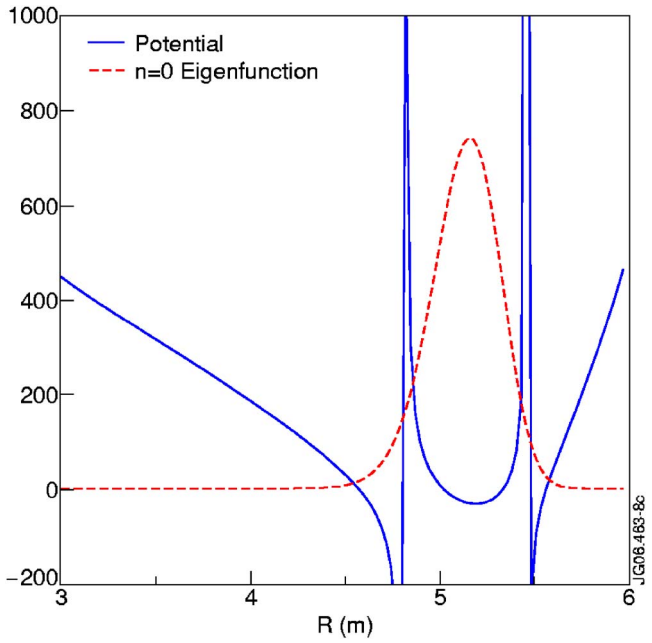

FIG. 8. (Color online) Full potential along with the z component of the electric field corresponding to the $p=0$ eigenfunction (plotted in arbitrary units) for $\kappa_T=0.5$, $N_\parallel^2=10000$, and $\omega=5.0579\times10^7$ rad s^{-1}. Note the spikes in this figure are a result of the mode conversion layer $\varepsilon_1=N_\parallel^2$.

IV. RADIAL STRUCTURE OF MODE CONVERSION LAYERS $\varepsilon_1(R)=N_\parallel^2$

In a single ion species plasma, ε_1 takes the following approximate form:

$$\varepsilon_1(R,\omega)\approx-\frac{\omega_{pi}^2}{\omega^2-\omega_{ci}^2(R)}, \tag{21}$$

and the mode conversion from the fast compressional Alfvén wave to the ion Berstein wave occurs at the $\varepsilon_1(R)=N_\parallel^2$ surface when thermal effects are included.[13] The mode conversion constitutes one of the main damping mechanisms for fast compressional Alfvén waves. For a single ion species plasma, Eq. (21) tells us that $\varepsilon_1>0$ only when $\omega<\omega_{ci}$, and so the plasma can be easily divided into regions where $\omega<\omega_{ci}$ is true, and hence where the mode conversion can occur.

For a two ion species plasma, such as D-T, ε_1 is given by the sum of two terms in Eq. (5) and so the situation is more complicated depending on the mode frequency ω. Seven different frequency regimes can then be identified, as Fig. 9 shows. Here the radial positions of the mode conversion layers are found in a STPP for different frequency regimes with a 50:50 D-T mix.

A. Regime 1

For this regime, $\omega<\omega_{cD},\omega_{cT}$, which means $\varepsilon_1(R)>0$ and so $\varepsilon_1(R)=N_\parallel^2$ mode conversion may be possible depending on the value of $N_\parallel^2$. Figure 10 shows an example of $\varepsilon_1(R)$ for a frequency in this regime; note that $N_\parallel^2$ will have to be of the order of 10^4 for the mode conversion surface to occur in the core of the plasma. It should also be noted that ε_1 does not go to zero at the inboard side of the torus, so there is a threshold $N_\parallel^2$ for the mode conversion to occur.

B. Regime 2

For this regime, $\omega_{cT\,\min}<\omega<\omega_{cD\,\min}$, where minimum values $\omega_{cT\,\min}$ and $\omega_{cD\,\min}$ are close to the magnetic axis (see Fig. 2). Depending on how close the frequency is to $\omega_{cD\,\min}$, we may or may not see mode conversion. Referring to Fig. 9, to the far left (e.g., $R<3m$), $\omega<\omega_{cD},\omega_{cT}$ and so $\varepsilon_1(R)>0$, and, as in regime 1, mode conversion may be possible depending on $N_\parallel^2$. As we approach $\omega\to\omega_{cT}$, $\varepsilon_1\to+\infty$. Just to

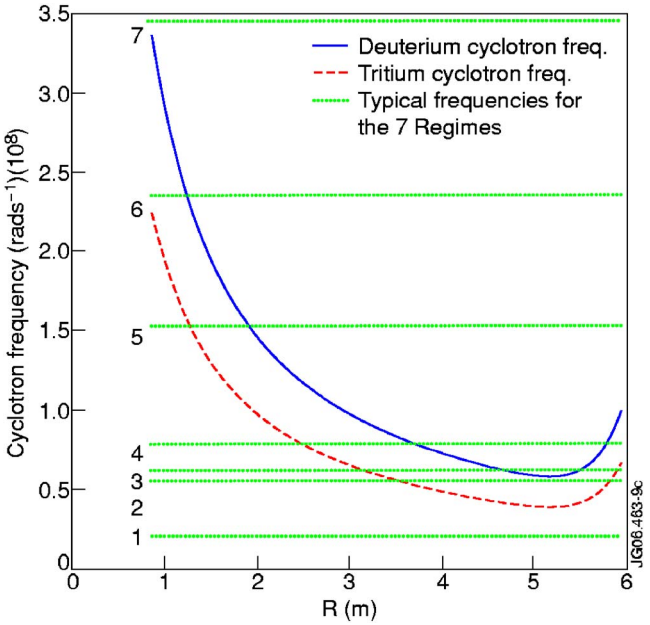

FIG. 9. (Color online) Cyclotron frequencies [dashed (T) and solid (D)] calculated using the magnetic field from Fig. 3 and typical frequencies (dotted) for regimes 1–7.

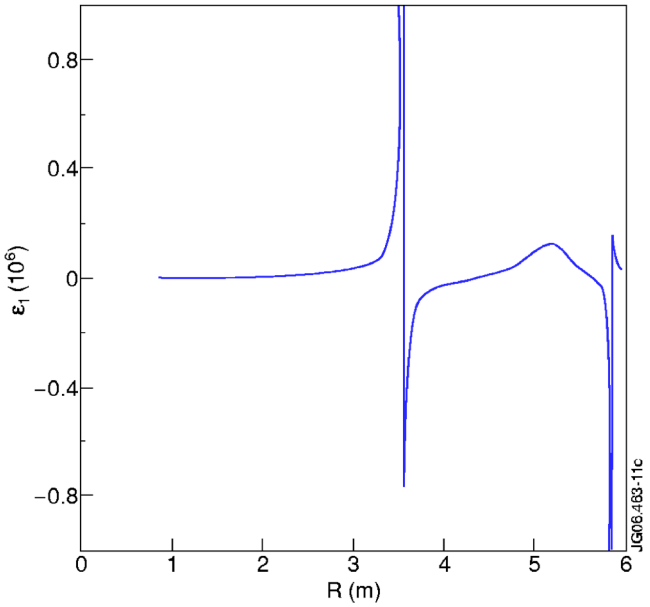

FIG. 11. (Color online) ε_1 for $\kappa_T=0.5$ and $\omega=5.5\times10^7$ rad s^{-1}.

the right of this singularity in $\varepsilon_1(R)$, where $\omega>\omega_{cT}$, one observes $\varepsilon_1<0$. Since $\omega<\omega_{cD}$ in this region, the deuterium term provides a positive contribution to ε_1. However, absolute values of ε_{1D} and ε_{1T} depend on $|\omega-\omega_{cD}|$ and $|\omega-\omega_{cT}|$. So unless $\omega-\omega_{cD\,\mathrm{min}}$ is small, this will not be enough to make the total ε_1 positive and so mode conversion will not occur. Figure 11 shows an example of where mode conversion is possible; note that there is no threshold $N_\parallel^2$ needed for resonance, since ε_1 goes continuously through zero around the magnetic axis. Figure 12 shows an enlarged section of Fig. 11.

C. Regime 3

For this regime, we see, referring to Fig. 9, the far left has the same behavior as regime 2 and Fig. 13 shows an example of this regime. As we pass through $\omega=\omega_{cT}$, as before $\varepsilon_1<0$, however ε_1 will change sign as the positive contribution from ε_{1D} becomes larger as $\omega\rightarrow\omega_{cD}$. Thus ε_1 will smoothly increase through zero, so that mode conversion will occur, with no $N_\parallel^2$ threshold. As the deuterium singularity is traversed, $\omega>\omega_{cD},\omega_{cT}$ and so there is a region where $\varepsilon_1<0$ and so no mode conversion. Finally, toward the outboard side of the plasma the reverse of what has just been

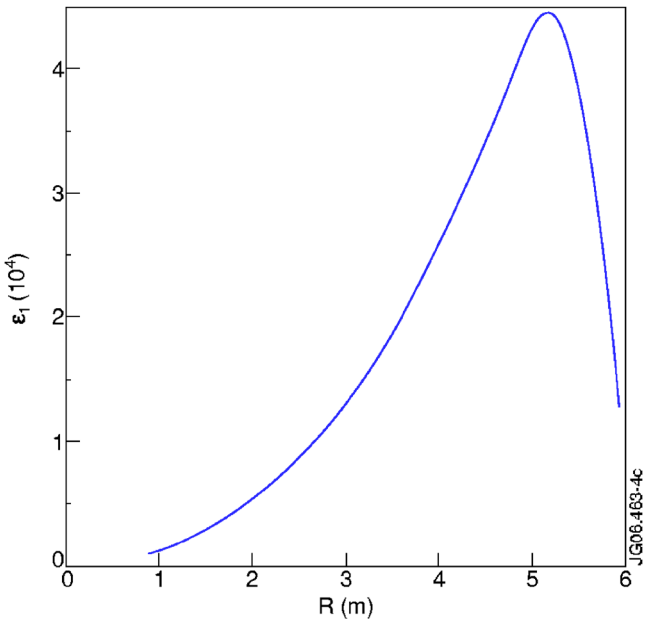

FIG. 10. (Color online) ε_1 for $\kappa_T=0.5$ and $\omega=2\times10^7$ rad s^{-1}.

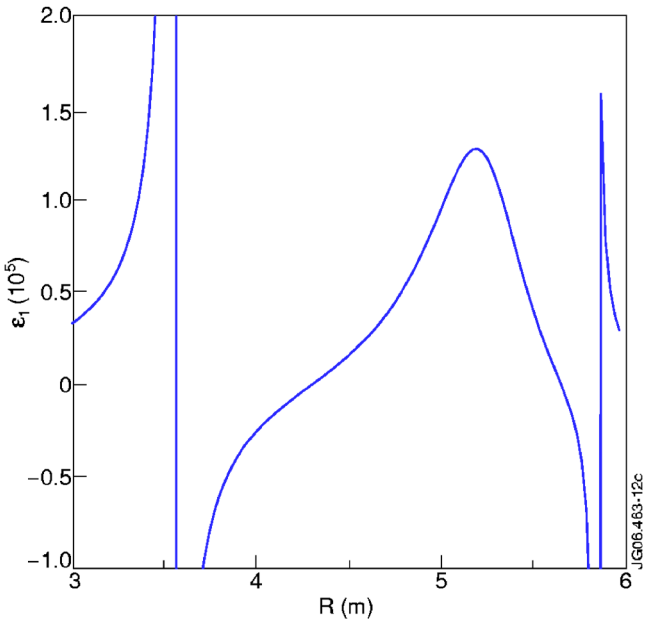

FIG. 12. (Color online) Enlarged section of Fig. 11.

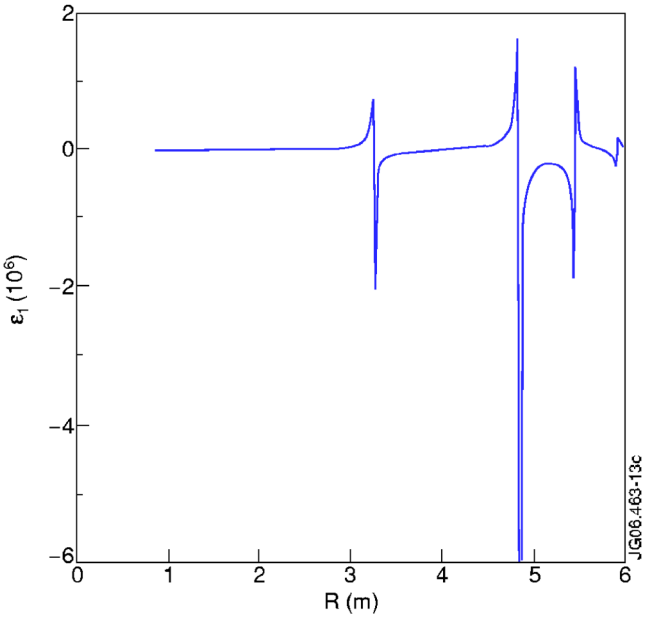

FIG. 13. (Color online) ε_1 for $\kappa_T=0.5$ and $\omega=6\times10^7$ rad s^{-1}.

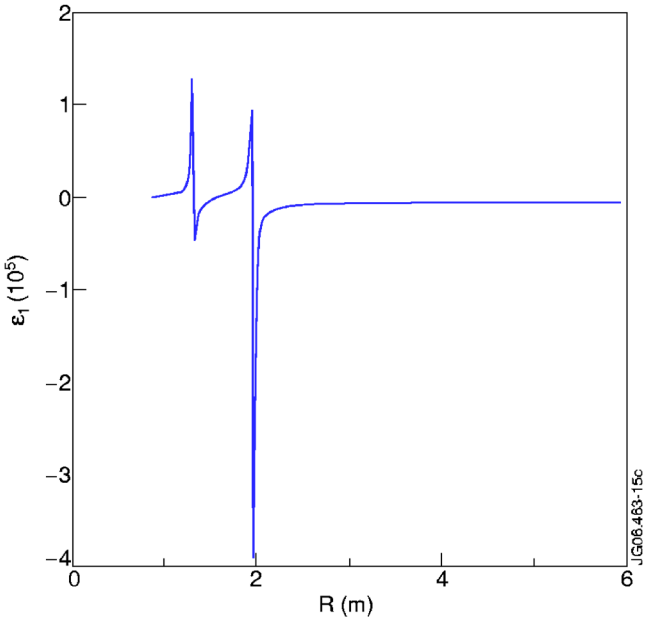

FIG. 15. (Color online) ε_1 for $\kappa_T=0.5$ and $\omega=1.5\times10^8$ rad s^{-1}.

described takes place, so that there will be one more definite mode conversion, and a conditional one depending on the value of $N_\parallel^2$.

D. Regime 4

This regime is almost identical to regime 3, the difference being there is no guaranteed mode conversion at the outboard side any more. Figure 14 shows an example of this regime, when resonance at the outboard side can occur. The absence of the outboard mode conversion can be due to $\omega > \omega_{cT}$ at the outboard side, so that there is no tritium singularity. This means that if the frequency is too high, then the negative contribution from ε_{1T} will not be enough to reduce ε_1 from very large positive values (just after $\omega=\omega_{cD}$) through zero. The implication then is that one may have mode conversion, however it depends on the value of $N_\parallel^2$ (there is now a threshold again).

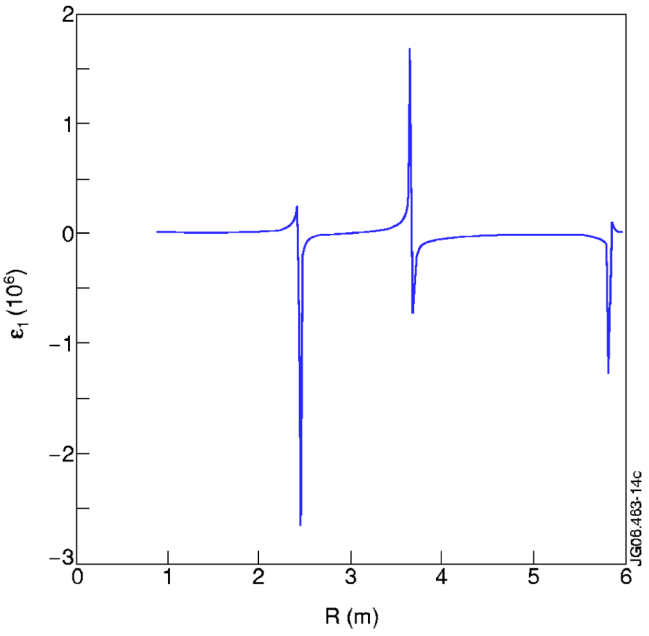

FIG. 14. (Color online) ε_1 for $\kappa_T=0.5$ and $\omega=8\times10^7$ rad s^{-1}.

E. Regime 5

Referring to Fig. 9, the mode conversion behavior has already been described in the previous regimes; the mode conversion is always present when $\omega_{cT}<\omega<\omega_{cD}$ and may be present at the inboard side. Note no mode conversion can occur at the outboard side anymore, since $\omega>\omega_{cD},\omega_{cT}$. Figure 15 shows an example of this regime.

F. Regime 6

This regime displays the same behavior at the inboard side as regime 4 at the outboard side. Resonance depends on how high the frequency is: if it is too high, then there will be a threshold value of $N_\parallel^2$, otherwise ε_1 decreases smoothly through zero and a guaranteed mode conversion occurs. Figure 16 shows an example of when mode conversion can occur.

G. Regime 7

Finally for this regime, $\omega>\omega_{cD},\omega_{cT}$, which means $\varepsilon_1<0$ and so no mode conversion is possible.

H. MHD spectroscopy of D-T concentration from EM modes in a STPP

By analyzing how the eigenfrequencies (calculated in Sec. III) vary as a function of D-T concentration and $N_\parallel$, one can determine whether an active frequency sweeping diagnostic, with an external antenna in the proper frequency range, could be used to determine the D-T concentration.[8] By matching the frequency of the externally launched wave to

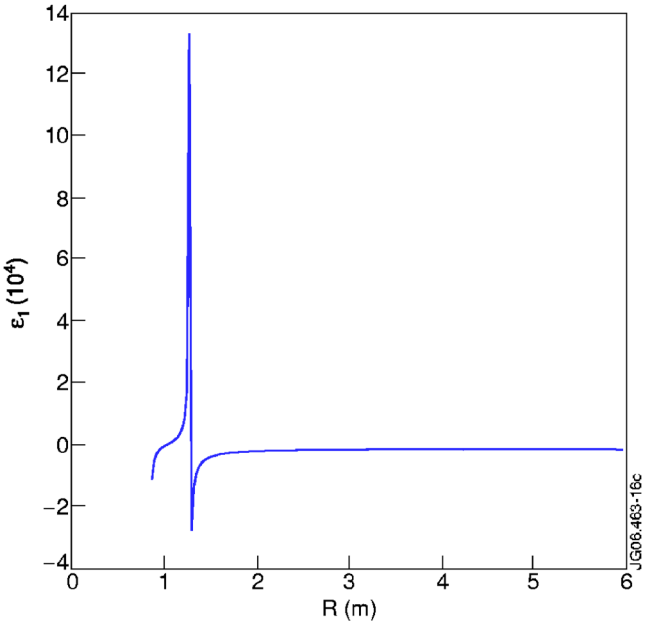

FIG. 16. (Color online) ε_1 for $\kappa_T=0.5$ and $\omega=2.3\times10^8$ rad s^{-1}.

that of the eigenmode, a resonant response of the plasma could be detected and thus indicate the D-T mix. We seek to find what value of $N_\parallel$ maximizes the change in mode frequency for a given change in D-T concentration (i.e., $d\omega/d\kappa_T$), since this makes the diagnostic technique most sensitive. If mode damping is weak enough, the width of the resonance peak will be small, and so diagnosing the D-T concentration will be more accurate. For this reason, we focus our analysis on the ω_1 eigenfrequency, since it can be seen from Fig. 7 that $\varepsilon_1=N_\parallel^2$ occurs far away from the region of mode localization. For ω_2, where we expect damping to be strong, ion-ion hybrid layer reflectometry may be a more appropriate diagnostic.[20] This will be discussed in Sec. IV I. Figure 17 shows the $p=0$ ω_1 eigenfrequencies as a function of κ_T and $N_\parallel^2$. One can see that Fig. 17 is largely monotonic, and so by choosing $N_\parallel^2=7000$ one is able to obtain a unique eigenfrequency for a given κ_T, and also maximize $d\omega/d\kappa_T$, and hence the sensitivity of the diagnostic. However, Fig. 17 shows that the sensitivity of $d\omega/d\kappa_T$ as a function of $N_\parallel$ is

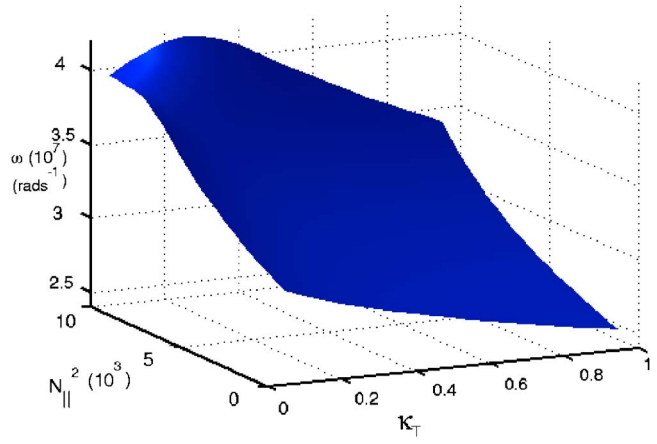

FIG. 17. (Color online) ω_1 as a function of κ_T and $N_\parallel^2$.

TABLE II. Couplet distances as a function of κ_T for $\omega=5.5\times10^7$ rad s^{-1} and $N_\parallel^2=10000$.

κ_T	$\delta(m)$	$\epsilon(m)$
0.2	2.453	—
0.33	0.6228	0.2209
0.5	0.2905	0.1103
0.4	0.1550	0.0649
0.66	0.1083	0.0507
0.71	0.0903	0.0471
0.75	0.0829	0.0478
0.77	0.0816	0.0517
0.8	0.0866	0.0605

not strong. This indicates that an external antenna probing the plasma may have a broad choice of $N_\parallel$ values. Also Table I shows that the frequency separation $\Delta\omega$ between modes with different radial mode numbers p, as well as frequency separation between different types of mode, is significant enough (more than $\Delta\omega/\omega\sim10\%$) in most cases, so that mode damping below this value would still be acceptable for identifying the resonance peaks with an external antenna.

I. Cutoff resonance couplet

We argued previously that $V=0$ was a necessary condition for the plasma to exhibit an eigenmode structure. When two such points exist, the plasma functions as a high-quality resonating cavity for the electromagnetic eigenmode (similar to quantum mechanics with a potential well). Also analogous with quantum mechanics is the tunneling phenomenon, where the wave exponentially decays into the region of the potential that it cannot exist in classically. If the distance between points where $V=0$ and $\varepsilon_1=N_\parallel^2$ (couplet distance) is smaller than the wavelength of our modes, then a cutoff resonance couplet can form enabling ion-ion hybrid layer reflectometry to be performed for measuring the plasma ion species mix (even in the case of launching microwave beams from the high field side).[20] In the case of EM eigenmodes, the formation of a couplet increases the wave damping and so decreases the accuracy of the EM antenna technique described in Sec. IV H. A calculation of the couplet distance is therefore required to identify the appropriate diagnostic.

We focus on frequencies in regime 2 from the last section, and define δ and ϵ to be the distance from the mode conversion layer to $V=0$ on the inboard and outboard side of the potential, respectively. By keeping $\omega=5.5\times10^7$ rad s^{-1} fixed, we vary the concentration of tritium by varying κ_T, and then vary $N_\parallel^2$ to see their effect on the couplet distance.

Figure 8 shows that the wavelength of our eigenmode is about 1 m, and from Tables II and III one can see that the couplet distances are (except in the case $\kappa_T=0.2$) shorter than one wavelength. This gives an indication that a reflectometry diagnostic similar to Ref. 20 may be used to detect the D-T mix. More specifically, Ref. 20 describes experiments on DIII-D where the ion species mixture ratio could be determined from waves launched from both the low- and high-field sides of the plasma. As long as the couplet distance was

TABLE III. Couplet distances as a function of $N_{\|}^2$ for $\omega=5.5\times10^7$ rad s^{-1} and $\kappa_T=0.5$.

$N_{\|}^2$	$\delta(m)$	$\epsilon(m)$
0	0.1240	0.0390
1000	0.1184	0.0375
2000	0.1132	0.0362
3000	0.1085	0.0350
4000	0.1047	0.0340
5000	0.1022	0.0335
6000	0.1022	0.0339
7000	0.1072	0.0359
8000	0.1240	0.0423
9000	0.1733	0.0611
10000	0.2905	0.1103

smaller than one wavelength, the wave could tunnel through the mode conversion layer and reflectometry could still be performed even from the high-field side.

V. CONCLUSION AND DISCUSSION

For high β STPP equilibria, it has been shown that the characteristic well in the equilibrium magnetic field acts as a resonating cavity for electromagnetic waves, forming discrete spectra of compressional Alfvén and ion-ion hybrid eigenmodes in the plasma core. The frequency and structure of these eigenmodes have been calculated using a "cold plasma" approximation, similar to Ref. 10, but with D-T mixture effects taken into account. Although high β plasmas require a kinetic description, the cold plasma approximation provides a first insight into the radial structure of the cutoffs and mode conversion positions over a broad range of $k_{\|}$ and frequencies. Inclusion of D-T effects in the calculation reveals a discrete spectrum of eigenfrequencies not only above the ion cyclotron frequency[10] but also in the ion-ion hybrid frequency range. Taking into account the dependence of the eigenfrequencies on the D-T concentration, we optimized this dependence with respect to $k_{\|}$ in order to obtain the maximum value of $d\omega/d\kappa_T$. The possibility of using the eigenmodes, found in this paper, as a diagnostic for measuring the D-T concentration, by observing α particle driven emission or probing the discrete spectrum with externally launched EM waves in the ion cyclotron frequency range, has been proposed. Furthermore, the radial position of mode conversion layers in a STPP geometry has been identified for various frequency regimes. This information is necessary for estimates of the mode damping and for further assessment of the feasibility of diagnostic techniques described in Refs. 8 and 20. Further development of the discrete spectrum in a STPP will include hot plasma effects, magnetic geometry boundary layer effects, and a realistic functional dependence of $k_{\|}$ on radius. Stability analysis will also be the subject of further investigation. This will involve a full calculation of the damping due to mode conversion, deuterium and tritium ion cyclotron damping, electron damping, along with a calculation of the alpha particle drive.

ACKNOWLEDGMENTS

We would like to acknowledge M. Hole for providing the STPP equilibrium data, and we thank T. Hender, S. C. Cowley, M. Coppins, and J. D. Martin for their support and encouragement.

This work was funded by Euratom and the UK Engineering and Physical Science Research Council. The views and opinions expressed herein do not necessarily reflect those of the European Commission.

[1] H. R. Wilson, G. Voss, J.-W. Ahn *et al.*, in *19th IAEA Fusion Energy Conference*, October, 2003 (IAEA, Lyon, France, 2002), No. FT/1–4.
[2] Y. K. M. Peng and D. J. Strickler, Nucl. Fusion **26**, 769 (1986).
[3] M. Gryaznevich, R. Akers, P. G. Carolan *et al.*, Phys. Rev. Lett. **80**, 3972 (1998).
[4] D. A. Gates, Phys. Plasmas **10**, 1659 (2003).
[5] B. Lloyd, Nucl. Fusion **43**, 1665 (2003).
[6] E. D. Fredrickson, Phys. Plasmas **10**, 2852 (2003).
[7] E. D. Fredrickson, N. N. Gorelenkov, and J. Menard, Phys. Plasmas **11**, 3653 (2004).
[8] T. Intrator, M. Vukovic, A. Elfimov, P. H. Probert, and G. Winz, Phys. Plasmas **3**, 1054 (1996).
[9] S. J. Buchsbaum, Phys. Fluids **3**, 418 (1960).
[10] M. V. Gorelenkova and N. N. Gorelenkov, Phys. Plasmas **5**, 4104 (1998).
[11] M. Brambilla, *Kinetic Theory of Plasma Waves* (Oxford Science, Oxford, 1998), p. 165.
[12] S. C. Hsu, M. Artun, and S. C. Cowley, Phys. Plasmas **3**, 266 (1996).
[13] A. I. Akhiezer, I. A. Akhiezer, R. V. Polovin, A. G. Sitenko, and K. N. Stepanov, *Plasma Electrodynamics Volume 1: Linear Theory* (Pergamon, New York, 1975), pp. 253 and 212.
[14] S. C. Cowley, P. K. Kaw, and R. M. Kulsrud, Phys. Fluids B **3**, 2066 (1991).
[15] R. Majeski, C. K. Phillips, and J. R. Wilson, Phys. Rev. Lett. **73**, 2204 (1994).
[16] Obtained from K. G. McClements, Phys. Plasmas **12**, 072510 (2005) (Ref. 21): H. R. Wilson, UKAEA Fusion Report No. FUS 271, 1994 (unpublished).
[17] L. D. Landau and E. M. Lifshitz, *Quantum Mechanics (Non-relativistic Theory)* (Elsevier, Amsterdam, 2005), p. 72.
[18] D. G. Swanson, Phys. Rev. Lett. **36**, 316 (1976).
[19] I. Monakhov, A. Bécoulet, D. Fraboulet, and F. Nguyen, Phys. Plasmas **6**, 885 (1999).
[20] G. W. Watson, W. W. Heidbrink, K. H. Burrell, and G. J. Kramer, Plasma Phys. Controlled Fusion **46**, 471 (2004).